Journal of Engineering Science and Technology Review 16 (2) (2023) 49 - 58

Research Article

JOURNAL OF
Engineering Science and Technology Review

www.jestr.org

Particle Flow Movement Behavior of Asphalt Pavement under Vehicle Load

Junhui Zhang, Xiaoyong Wu*, Shiteng Rong, Lizhe Diao, and Junzhan Qi

Shijiazhuang Hongye Traffic Construction Supervision Co. LTD, Shijiazhuang 050081, China

Received 5 January 2023; Accepted 3 April 2023

Abstract

The damage to asphalt pavement is closely related to the movement behavior of various material particles in the asphalt mixture under the load of a vehicle. A 2-degree-of-freedom 1/4 vehicle model was constructed to analyze the movement behavior of particles in each structural layer of asphalt pavement. The mechanical behavior of various pavement materials was described by the constitutive relationship of the parallel bond model and contact bond model. The mesoparameters of each material were obtained through uniaxial compression tests. A 3D discrete element model of asphalt pavement was constructed, and the movement of the vehicle load was simulated by using the fish program. Results show that the asphalt pavement structure model can be constructed in accordance with discrete element theory, and the error between the calculated results of the discrete element model and the measured results is within 7%. The vertical velocity of the pavement structural layer particles is the largest, and the transverse velocity is the smallest. The translational velocity of particles in the upper layer is much higher than that in the middle layer, and the translational velocity of particles in the base layer is the least. The vertical contact force between particles is the largest, followed by the longitudinal contact force, and the transverse contact force is the least. These conclusions provide a valuable reference for similar asphalt pavement engineering.

Keywords: Asphalt pavement, Vehicle load, Granular flow, Mesoscopic parameters, Mechanical response

1. Introduction

Asphalt pavement has been increasingly used on highways in China due to its many advantages. However, the increasingly severe climate environment, serious overload, and differences in construction technology and ground material can limit the service life of the asphalt pavement, resulting in frequent maintenance and serious diseases later on. With the progress of scientific research and continuous improvement of construction technology and mechanization, many issues related to asphalt pavement have been effectively solved and controlled. However, asphalt pavement can develop cracks, deformation, and other diseases under the rolling effect of vehicle load, which can seriously shorten its service life [1-2].

In the early stage of research on asphalt mixture damage, laboratory tests were the predominant research method, and many achievements have been made on the basis of these tests. However, although laboratory tests consume time and cost, they can only be conducted from a macro perspective, making it difficult to reveal the mechanical mechanism of asphalt cracking and the structural evolution of asphalt from macroscopic perspectives and to identify the source of damage. With the development of technology, many scholars have introduced the finite element method (FEM) into the analysis of asphalt pavement. The introduction of FEM has brought a new research perspective and led to many achievements. However, with the deepening of research, the shortcomings of FEM numerical simulation in the simulation of asphalt mixture as a multidirectional composite material have become increasingly evident. For example, FEM cannot describe important characteristics of asphalt mixture, such as porosity, and it is not suitable for simulating large deformation and discontinuous deformation. By contrast, the discrete element method (DEM) avoids the continuity assumption in FEM and is suitable for simulating large and discontinuous deformation. Therefore, the use of DEM in the study of asphalt mixture has incomparable advantages over other research methods. DEM in asphalt mixture research has achieved remarkable progress in the last decade.

Asphalt mixture is composed of coarse aggregate, fine aggregate, asphalt, and admixtures. When vehicle load is applied, the characteristics of asphalt mixture are heterogeneous and discontinuous. Consequently, the damage of asphalt mixture is closely related to the mechanical relationship between various materials. Many experts aim to reveal the principle of pavement damage through fracture mechanics, continuous damage, and other methods, but the ideal result has not been achieved. With a deepening understanding of the internal structure of asphalt mixture, the use of fine/micro mechanics theory to analyze asphalt pavement damage has become a hot topic [3].

Therefore, studying the movement behavior of particles in each structural layer of asphalt pavement is of it is of great theoretical importance and practical value. In addition, the asphalt pavement structure model based on discrete element theory can be used to simulate and analyze the mechanical behavior of the vehicle and the road surface.

2. State of the art

In the theory of micromechanics, mixtures are considered to be composed of particle flows with different shapes and

*E-mail address: 15030150080@139.com
ISSN: 1791-2377
doi:10.25103/jestr.162.07

sizes, with a certain mechanical relationship between these particles. When an external load is applied, the motion state of the particles is related to the macroscopic mechanical behavior of the mixture. The movement behavior of particles has been studied by many experts [4, 5]. Zhang et al. [6] conducted dynamic shear rheology (DSR) trials with four filler concentrations of asphalt slurry and validated the DSR experiments with 3D DEM to obtain additional master curves for different filler concentrations of asphalt slurry. Arshadi and Bahia [7] analyzed the mechanical contact behavior between asphalt mixture particles and adopted unit scale amplification and homogenization theory to increase the calculation cost based on image multiscale modeling method. Wang et al. [8, 9] analyzed the deformation mechanism of aggregate in the process of specimen loading from the perspective of micromechanics and studies the influence of temperature on aggregate particles. A virtual model of AC-13 asphalt mixture was built on the basis of discrete element theory.

To describe the mechanical behavior of particles more accurately, various discrete element modeling methods of asphalt mixture have been studied. Chen et al. [10] built 2D and 3D models under different conditions to study the dynamic modulus and phase angle of asphalt mixture, while considering the mix ratio and spatial distribution of mixture, and the properties of coarse aggregate. Miao et al. [11] investigated the average contact number and interaction forces of aggregate particles of different sizes using the DEM to analyze the skeletal structure of the aggregate mixture and the function of the aggregate particles from a microstructural point of view. Li et al. [12] proposed an algorithm that generates 3D assemblies by splitting the plane of a rectangular model and verified its reasonableness by comparing the results of uniaxial compression tests.

Ding et al. [13] established skeleton particle structures with different states based on DEM with an imaging measurement system to analyze the mechanical effects of different shapes of particles on asphalt mixture. Two-dimensional images were obtained, and key morphological features of different skeleton particles were analyzed to predict the frictional resistance within the skeleton. The accuracy of these modeling methods was compared. Buttlar and You [14] proposed a microfabric discrete element modeling method for modeling the microstructure of asphalt concrete. To study the performance of asphalt mixture containing thin or flat particles, Wang et al. [15] obtained 3D images with a laser scanner and constructed a discrete element model of asphalt mixture based on the position of particles. The mechanical effects of different shapes of particles on asphalt mixture were analyzed. Chang et al. [16] utilized the DEM to construct a model of asphalt mixture (AC-13, SMA-13, and OGFC-13). They analyzed the relationship between the force chains of particles under external loads and studied the change law of strong and weak chains in detail. Many scholars have studied small asphalt mixture specimens, and the mechanical behavior of particles under static load is analyzed. However, the force acting on the asphalt pavement is mainly due to the dynamic load of vehicles [17, 18]. Therefore, certain differences are observed between the asphalt pavement status obtained from the research and the actual status. Few studies have investigated the combination of vehicle dynamic load and road surface based on DEM. Hence, this study has certain research importance [19-22].

A 2-degree-of-freedom (DOF) 1/4 vehicle model was established in this study to address the aforementioned problems. The mechanical behavior between particles was described by using the relationship between parallel bonding and linear contact. The mesoscopic parameters of asphalt mixture were obtained experimentally. The fish language in PFC software was used to simulate the movement of the vehicle load. The variation law of particle movement velocity and contact stress between particles in each structural layer of asphalt pavement was analyzed.

The rest of this study is organized as follows. Section 3 describes the construction of numerical model methods. Section 4 presents the results and discussion, and Section 5 summarizes the conclusions.

3. Methodology

3.1 Vehicle model construction

Generally, a vehicle consists of a vehicle body, a spring vibrator, and a damper. For simplification of calculation, a 2-DOF 1/4 vehicle model was established, as shown in Fig. 1.

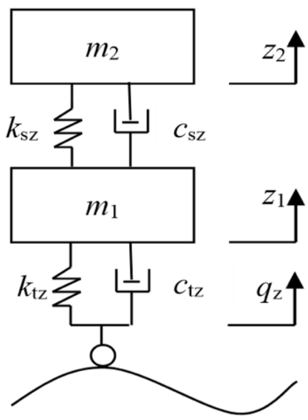

Fig. 1. 1/4 vehicle-road interaction dynamic model.

As shown in Fig. 1, m_1 and m_2 represent the tire mass and vehicle body mass, respectively. z_1 is the tire vertical dynamic displacement. z_2 is the vertical dynamic displacement of the vehicle body. k_{sz} is the stiffness coefficient of the vehicle suspension. k_{tz} is the vertical stiffness coefficient of the tire. c_{sz} is the damping coefficient of the car suspension. c_{tz} is the vertical damping coefficient of the tire, and q_z is the vertical roughness of the road surface. The vehicle model used is the Ford Granada model, and its parameters are shown in Table 1.

With the road roughness as the excitation, the vertical dynamic equation between the vehicle and the road surface can be expressed as follows [23]:

$$\begin{cases} m_2\ddot{z}_2 + c_{sz}\left(\dot{z}_2 - \dot{z}_1\right) + k_{sz}\left(z_2 - z_1\right) = 0 \\ m_1\ddot{z}_1 - c_{sz}\left(\dot{z}_2 - \dot{z}_1\right) - k_{sz}\left(z_2 - z_1\right) + c_{tz}\left(\dot{z}_1 - \dot{q}_z\right) + k_{tz}\left(z_1 - q_z\right) = 0 \end{cases} \tag{1}$$

The dynamic force produced by the vehicle on the road surface can be solved in accordance with the contact relationship between the tire and the road surface.

$$F_d = c_{tz}\left(\dot{z}_1 - \dot{q}_z\right) + k_{tz}\left(z_1 - q_z\right) \tag{2}$$

Table 1. Parameters of vehicle models

Vehicle body parameters	Value
Unsprung mass m_1 (kg)	40.5
Sprung mass m_2 (kg)	1380
Suspension stiffness coefficient k_s (kN·m^{-1})	17
Suspension damping coefficient c_s (kN·s·m^{-1})	1.5
Tire stiffness coefficient k_t (kN·m^{-1})	192
Tire damping coefficient c_t (N·s·m^{-1})	850

The load on the road surface is given by:

$$F = Mg + F_d \tag{3}$$

where, M_g is the static force of the vehicle itself. F_d is the dynamic force on the road surface. F is the resultant force on the road surface.

The 1/4 vehicle model was established using Matlab /Simulink software. With white noise as vehicle excitation (B-grade pavement, vehicle velocity v = 20 m/s), the load on the pavement was calculated (Fig. 2).

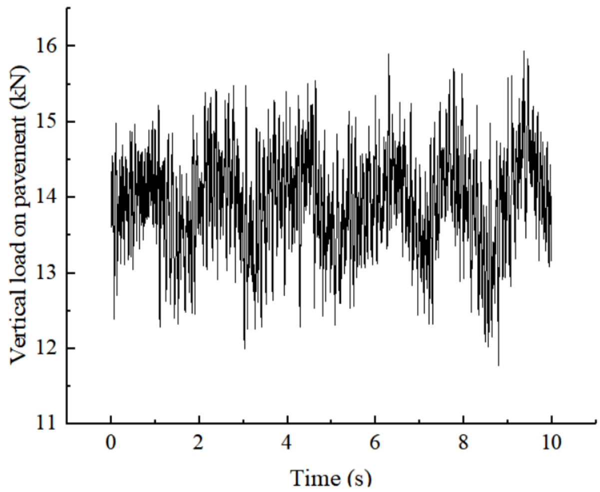

Fig. 2. Vertical load on the pavement by tires.

3.2 Asphalt pavement model

3.2.1 Constitutive relation of pavement material

The discrete element model is composed of many particles with inhomogeneous size. For each additional time step under an external load, all particles need to be recalculated, which takes a long time. A small asphalt pavement material model (0.5 m × 0.3 m × 0.3 m) was established in this study to reduce the amount of calculation, as shown in Fig. 3. The thickness of each pavement structural layer is listed in Table 2.

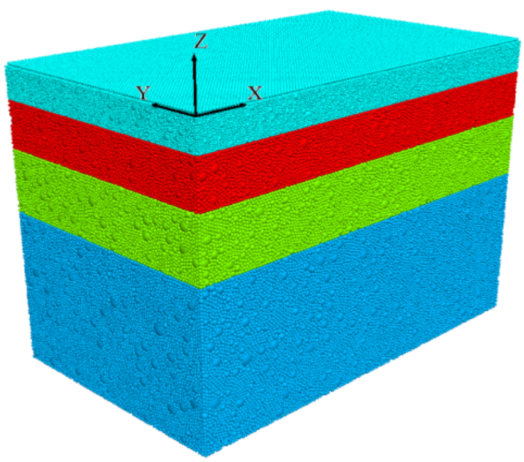

Fig. 3. Discrete element model of asphalt pavement.

Table. 2. Thickness of each pavement structural layer.

Material	Thickness (cm)	Structural layer
AC-13	4	Upper layer
HMAC-20	6	Middle layer
ATB-25 grade asphalt macadam	8	Lower layer
Cement stabilized macadam	18	Base layer

In accordance with stochastic theory, the particles of each structural layer were generated on the basis of the actual mix ratio. Coarse aggregate particles (greater than 2.36 mm) were used as the skeleton structure, and fine aggregate particles (less than 2.36 mm) filled the space of the skeleton. The interparticle force of cement-stabilized macadam was simulated by the bond model, and the interparticle force of the structural layer was simulated by the parallel bond model. The constitutive relation of the parallel bonding model is shown in Fig. 4.

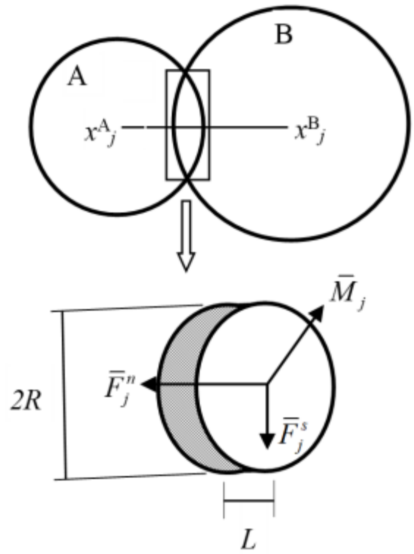

Fig. 4. Constitutive relation of the parallel bond model.

As shown in Fig. 4, x^A_j and x^B_j represent the center of the particle, $2R$ is the diameter of the contact model, L is the length, $\bar{M}_j$ is the moment of the contact model, $\bar{F}^n_j$ is the normal force, and $\bar{F}^s_j$ is the tangential force, The model shown in Fig. 4 is represented as follows:

$$\bar{F}_j = \bar{F}^n_j + \bar{F}^s_j \tag{4}$$

$$\bar{M}_j = \bar{M}^s_j + \bar{M}^n_j \tag{5}$$

When the external load is applied, the particle will produce a certain displacement, and the following mechanical relationship will exist.

$$\Delta\bar{F}^n_j = -\bar{k}_n H \Delta u_n \tag{6}$$

$$\Delta\bar{F}^s_j = -\bar{k}_s H \Delta u_s \tag{7}$$

$$\Delta\bar{M}^n_j = -\bar{k}_n I \Delta\theta_n \tag{8}$$

$$\Delta \bar{M}_j^s = -\bar{k}_s I \Delta\theta_s \tag{9}$$

$$\bar{k}^n = \frac{\bar{k}_n^A \bar{k}_n^B}{\bar{k}_n^A + \bar{k}_n^B} \tag{10}$$

$$\bar{k}^s = \frac{\bar{k}_s^A \bar{k}_s^B}{\bar{k}_s^A + \bar{k}_s^B} \tag{11}$$

where, H is the area of the contact model. I is the moment of inertia. Δu_n is the displacement along the normal direction. Δu_s is the displacement along the tangential direction. $\Delta\theta_n$ is the normal rotation angle. $\Delta\theta_s$ is the tangential rotation angle. $\bar{k}_n$ is the resultant stiffness in the normal direction. $\bar{k}_s$ is the resultant stiffness in the tangential direction.

At a certain time t, the forces and moments in the model are as follows:

$$\bar{F}_j^n(t) = \left|\bar{F}_j^n(t - \Delta t)\right|_n + \Delta\bar{F}_j^n \tag{12}$$

$$\bar{F}_j^s(t) = \bar{F}_j^s(t - \Delta t) + \Delta\bar{F}_j^s \tag{13}$$

$$\bar{M}_j^n(t) = \left|\bar{M}_j^n(t - \Delta t)\right|_n + \Delta\bar{M}_j^n \tag{14}$$

$$\bar{M}_j^s(t) = \bar{M}_j^s(t - \Delta t) + \Delta\bar{M}_j^s \tag{15}$$

The normal stress is given by:

$$\sigma = \bar{F}_j^n / H + \bar{M}_j^s \cdot R / I \tag{16}$$

The tangential stress is given by:

$$\tau = \bar{F}_j^s / H \tag{17}$$

Cement-stabilized macadam was used as the base material, but its performance under external load is brittle. Therefore, the linear bond model was used to reflect the mechanical characteristics of cement-stabilized macadam. The calculation process of the contact bonding model is the same as that of the parallel bonding model, except that it cannot withstand the moment ($\bar{M}_j = 0$). The constitutive relationship of each structural layer of the road surface is shown in Fig. 5.

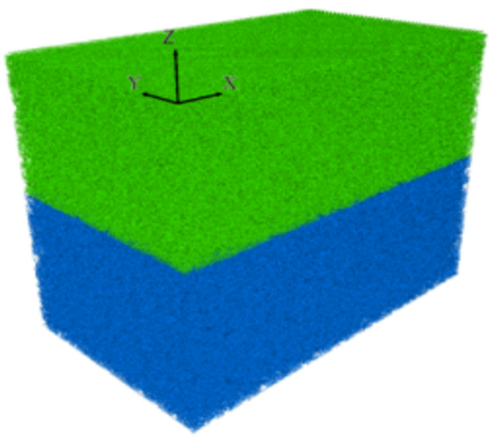

Fig. 5. Distribution of pavement material constitutive relation.

As shown from Fig. 5, the green part represents the parallel bonding model (the upper layer, the middle layer, and the lower layer), and the blue part represents the linear contact bonding model (the base layer).

3.2.2 Determining meso-parameters of pavement materials

When discrete element theory is used to calculate the mechanical behavior of materials, the mesoparameters of materials must be determined in accordance with the constitutive relation. The macroscopic parameters of materials cannot be used in discrete element calculations. However, a certain connection exists between macroscopic parameters and mesoparameters based on the breakage principle of materials [24, 25]. The discrete element model was constructed on the basis of stochastic theory. The mesoparameters calculated by different methods are relatively different. Therefore, great controversy exists among scholars regarding the mesoparameters of the material. In this study, Burger's model and trial-and-error method were used for asphalt mixtures. In accordance with the Itasca Consulting Group reference, the stress–strain time-history curve of micromechanics was fitted by using a trial-and-error method. The mesoparameters of various materials were obtained [26-28].

The numerical simulation of uniaxial compression failure test of AC-13 asphalt mixture is shown in Fig. 6. The uniaxial compressive failure test of asphalt mixture under standard conditions is shown in Fig. 7 [29]. As shown in Figs. 6 and 7, the cracking form of the asphalt mixture in the model is similar to that in the experiment.

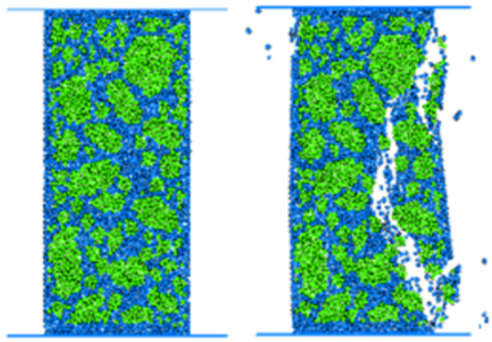

Fig. 6. Failure of AC-13 asphalt mixture under uniaxial compression.

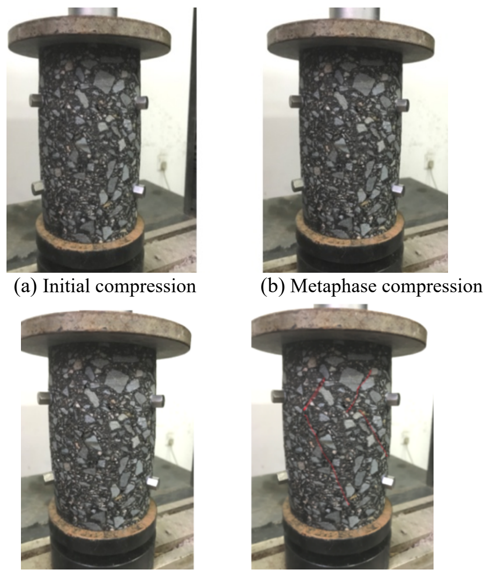

(a) Initial compression (b) Metaphase compression
(c) End of compression (d) Crack at end of compression

Fig. 7. Standard uniaxial compression test of AC-13 asphalt mixture.

The comparison between the experimental data of stress and strain of AC-13 asphalt mixture and its simulated data is shown in Fig. 8. The variation trend of the experimental data is similar to that of the model data, and the error of their maximum stress value is 7.5%. This finding shows that the mesoparameters of AC-13 asphalt mixture obtained by this method are feasible to a certain extent. The microscopic parameters of other pavement materials in this study were also obtained by the uniaxial compression test. The microscopic parameters of various pavement materials are shown in Tables 3 and 4.

Table 3. Meso-parameters of the parallel bonding model.

Structural layer	Particle density ($kg \cdot m^{-3}$)	Ratio of normal to tangential stiffness	Normal strength of parallel bond model (MPa)	Cohesive force of the parallel bonding model (MPa)	Elastic modulus of particles (MPa)	Particle radius (mm)
Upper layer	2700	0.8	5	6	520	1.18-8
Middle layer	2700	0.8	5	6	730	2.00-13.25
Lower layer	2700	1	6	5	400	2.00-15.75

Table. 4. Meso-parameters of the contact bonding model.

Structural layer	Particle density ($kg \cdot m^{-3}$)	Ratio of tensile to shear stiffness	Tensile strength of contact bond (MPa)	Shear strength of contact bond (MPa)	Elastic modulus of contact bond (MPa)	Particle radius (mm)
Base layer	2400	1	1	5	600	2.00-15.75

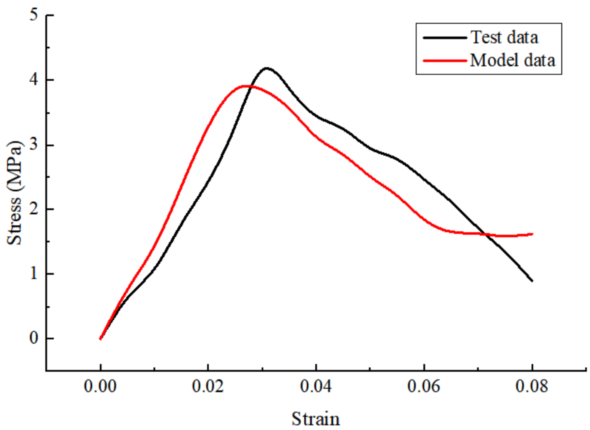

Fig. 8. Comparison of the stress-strain data of AC-13 asphalt mixture.

3.3 Movement of vehicle load

Assuming that the contact surface between the vehicle load and pavement is a rectangle (Fig. 9), the length d of the rectangle is expressed by Eq. 18. The particles on the rectangular surface uniformly carry the vehicle load. The vehicle load stays at the initial position at for a time interval Δt, then moves forward a distance l and stops at the new position at time Δt. Next, the vehicle load moves forward again for a distance of l and stops at the new position at time Δt. The three stages complete the movement process of the vehicle load.

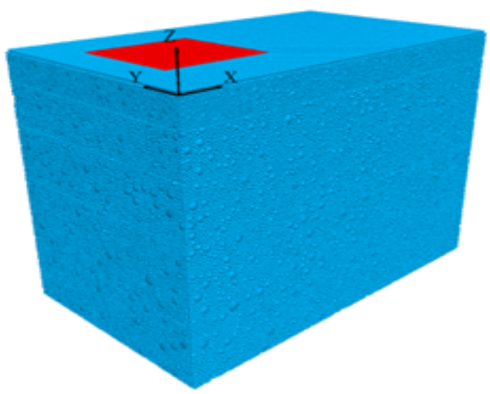

Fig. 9. Vehicle load acting on the road surface.

The length d of the rectangular side is given by:

$$d = \sqrt{P / p} \tag{18}$$

where, P is the vehicle load, p is the tire pressure. The value is 0.25 MPa.

The time interval Δt of load stagnation is given by:

$$\Delta t = 3.6 l / v \tag{19}$$

where, l is the distance the vehicle moves each time, $l = 4$ mm. v is the speed of vehicle movement, $v = 20$ m/s.

The time step n calculated by the model is given by:

$$n = \Delta t / \Delta t_0 \tag{20}$$

where, Δt_0 is the time step of the calculation.

4. Results analysis and discussion

4.1 Model validation

The vertical displacement and shear strain of each structure layer in the discrete element model were calculated in accordance with the moving mode of the vehicle load. This process was performed to verify the accuracy of the discrete element model. The results were verified by experiment due to the scarcity of literature using the DEM to calculate vehicle–road interaction. Strain gauges and displacement gauges are embedded in each structural layer of the roadbed and pavement of an expressway (Fig. 10). The structural layer of the actual pavement is the same as that of the discrete element model. The vertical displacement and shear strain are compared in Figs. 11 and 12.

(a) Sensor embedding of each structural layer of the road surface

(b) Observation of road surface response

Fig. 10. Observation of actual road surface.

The time-history curve of vertical displacement in the discrete element model is shown in Fig. 11(a). The time-history curve of vertical displacement measured on the actual pavement is shown in Fig. 11(b).

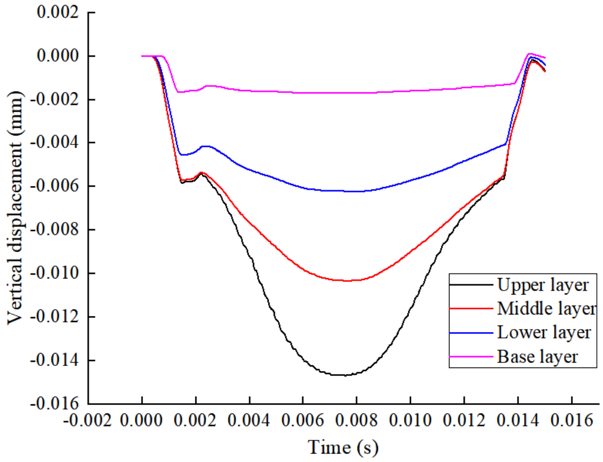

(a) Displacement curve in each layer of structure

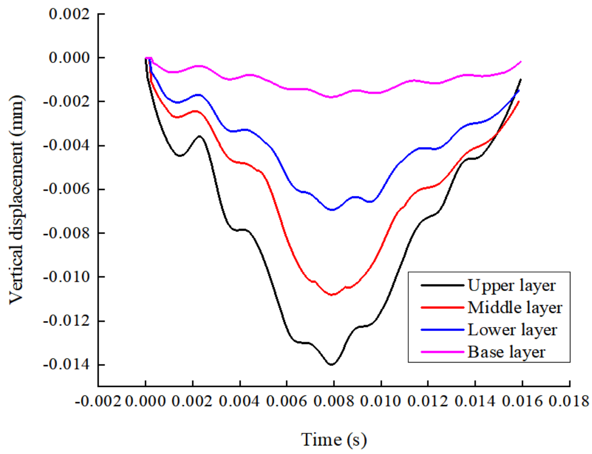

(b) Vertical displacement curve in the actual road surface

Fig. 11. Comparison of vertical displacements in each structural layer.

The longitudinal shear strains at the bottom of the asphalt layer at speeds of 50 and 70 km/h are shown in Figs. 12(a) and 12(b), respectively.

As shown in Figs. 11 and 12, the variation trend of vertical displacement/shear strain calculated by the discrete element model is similar to the measured results of pavement structure under vehicle load. The error between the simulation results and the measured results is less than 7%. The discrete element principle can be used to solve the response of the pavement structure layer, and the data obtained have a certain degree of accuracy. Moreover, the vertical displacement curve of the discrete element model is relatively smooth.

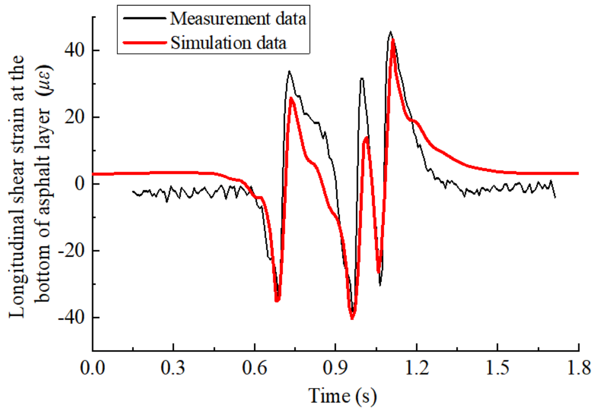

(a) Longitudinal shear strain at the bottom of asphalt layer at 50km/h

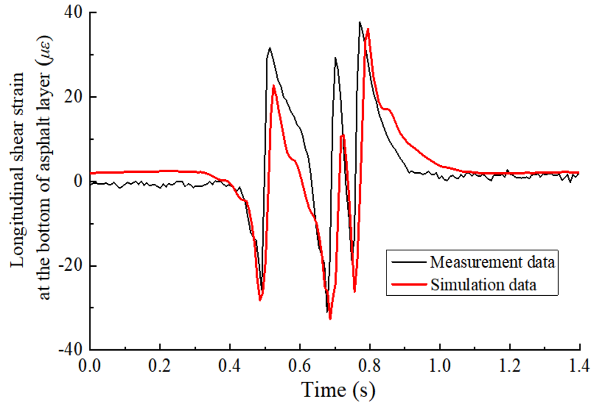

(b) Longitudinal shear strain at the bottom of asphalt layer at 70km/h

Fig. 12. Comparison of longitudinal shear strain at the bottom of asphalt layer.

4.2 Translational velocity of particles in each structural layer of asphalt pavement

The horizontal, longitudinal, and vertical translational velocities of particles at the midpoint of each layer are extracted to study the translational velocity of particles in each structural layer of the road surface. The particle velocities are shown in Figs. 13 to 15.

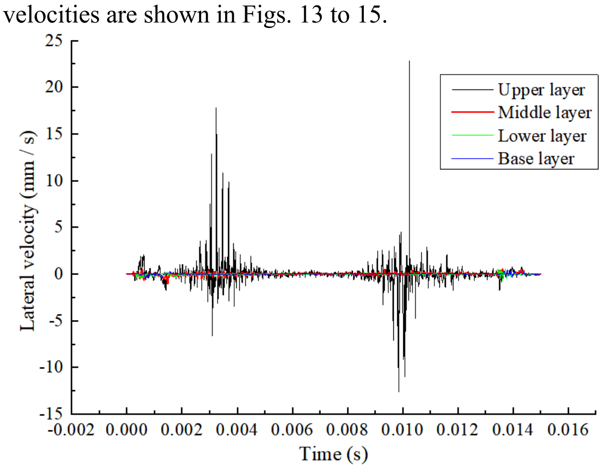

Fig. 13. Time history curve of particle lateral velocity.

Fig. 13 shows a comparison of the lateral movement velocities of particles in each structural layer. All particles in the road surface move laterally under the action of the vehicle load. The upper layer particles have the highest velocity, whereas the bottom particles have the lowest. The lateral velocity of the upper layer is 10-15 times greater than that of the middle layer. The lateral velocity of the middle layer is 2-3 times greater than that of the lower layer. The lateral velocity of the lower layer is 1.0-1.8 times greater than that of the base layer. These data show that the lateral velocity of particles decreases with the increase in the depth of the structural layer. When the vehicle approaches a particle, the lateral velocity of the particle increases. When the vehicle completely presses the particle, the lateral velocity of the particle decreases. When the vehicle leaves the observation point, the lateral velocity of the particle increases.

The time history curve of the longitudinal movement velocity of particles is shown in Fig. 14. All particles in the road surface move longitudinally at a certain velocity under the vehicle load, and the curve is symmetrical. The upper layer particles are the most active, with a maximum moving velocity of -33.3 mm/s to 29.5 mm/s. The velocity of longitudinal movement of the particles in the upper layer is much higher than that of the particles in the other structural layers. When the vehicle approaches or leaves the observation point, the particle velocity reaches a peak. When the vehicle completely compacts the road surface, the particles velocity appears positive. The velocity of particles in the middle layer is much smaller than that of the upper layer, with a maximum velocity of 2.4 mm/s when the vehicle completely compacts the road surface. The movement of the lower layer and base layer particles is similar. These data show that the particle velocity gradually decreases with the increase in the depth of the pavement structural layer. The change in the velocity of upper layer particles is the most significant.

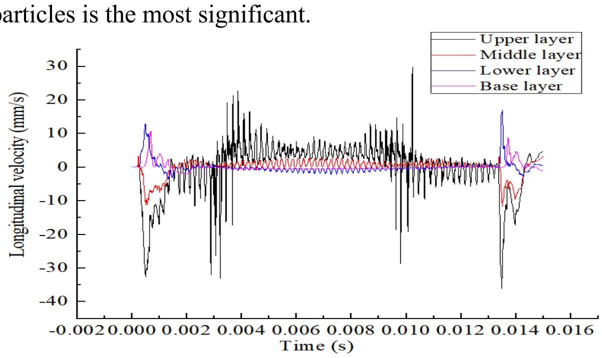

Fig. 14. Time history curve of longitudinal velocity.

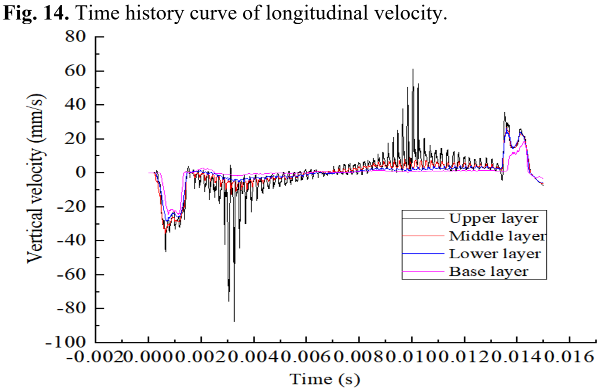

Fig. 15. Time history curve of vertical velocity.

As shown in Fig. 15, the particles of each structural layer of the road surface produce a certain vertical velocity under the vehicle load, and the curve of the vertical velocity is antisymmetric. The particles in the upper layer are the most active and have the highest vertical velocity (-87.63 to 60.7 mm/s). When the vehicle load approaches the observation point, the vertical velocity of the particles becomes negative. When the vehicle leaves the observation point, the vertical velocity becomes positive. When the vehicle completely presses the observation point, the particle velocity is smaller. The velocity of particles when the vehicle approaches the observation point is greater than when the vehicle leaves the observation point. The velocity of particles in the middle surface layer is much smaller than that of the upper layer, and their vertical velocity ranges from -12.2 mm/s to 8.34 mm/s. The vertical velocity of the lower layer particles ranges from -4.35 mm/s to 3.85 mm/s. The base particles have the minimum vertical velocity.

4.3 Rotation speed of particles in each structural layer of asphalt pavement

The rotational velocities of particles along the *X*, *Y*, and *Z* axes are extracted specially to study the rotation of particles under vehicle load. The rotational velocity of particles is shown in Figs. 16 to 18.

As shown in Fig. 16, the particles of each structural layer of the road surface rotate around the *X* axis, and the curve of their rotation velocity is symmetrically distributed. Positive and negative rotational velocities are observed, indicating that the particles oscillate back and forth about the *X* axis. The rotational velocity of the upper layer particles is the highest, ranging from -0.31 rad/s to 0.3 rad/s. The rotational velocity of particles in the middle layer is much smaller than that of the upper layer. The rotational velocity of the base layer particle is the minimum. These data show that the rotational velocity of particles decreases with the increase in the depth of the pavement structure layer. When the vehicle completely compacts the observation point, the particle rotation velocity is the minimum.

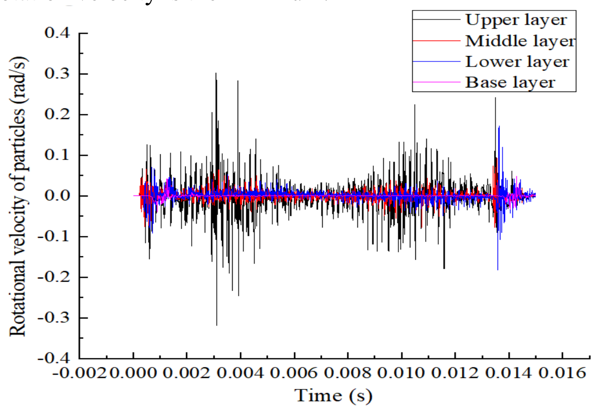

Fig.16. Rotation velocity of particles around the *X* axis.

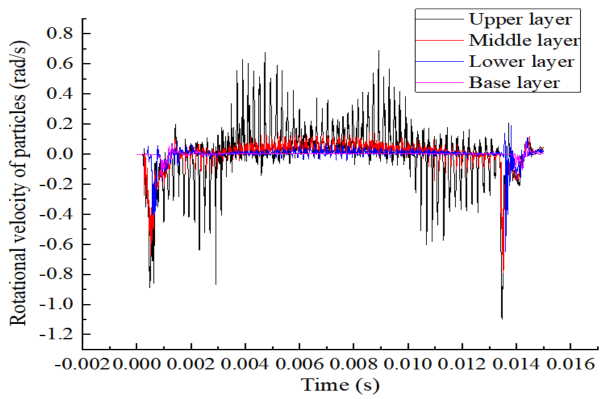

Fig. 17. Rotation velocity of particles around the *Y* axis.

Fig. 17 shows the rotation velocity of pavement structural layer particles around the *Y* axis under the action of vehicle load. When the vehicle approaches the observation point, the rotational velocity of particles in each structural layer is negative, with a maximum value of -0.87 rad/s. When the vehicle completely compacts the observation point, the rotational velocity of particles in each structural layer becomes positive, with a maximum value of 0.69 rad/s. The rotation velocity is minimum in the middle period. When the vehicle leaves the observation point, the rotational velocity of the particles becomes negative. The rotation velocity of particles in the middle layer is smaller than that of the upper layer, and its rotation trend is similar to the upper layer. The rotation velocity of the bottom particles is the smallest.

As shown in Fig. 18, the rotation velocity of the particles of each structural layer of the road surface around the *Z* axis is generated under the action of the vehicle load. The curve of rotational velocity is distributed symmetrically. Positive and negative rotational velocities are observed, indicating that the particles oscillate back and forth about the *Z* axis. The rotation velocity of the upper layer is the highest, ranging from -0.11 rad/s to 0.12 rad/s. The rotation velocity of particles in the middle layer is much smaller than that in the upper layer. The rotation velocity of base particle is the least. When the vehicle completely compresses the observation point, the rotation velocity of the particles is the smallest.

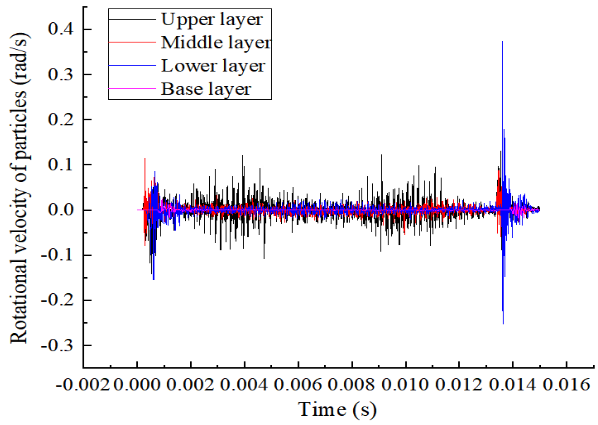

Fig. 18. Rotation velocity of particles around the *Z* axis

4.4 Force of particles in each structural layer of asphalt pavement

The transverse, longitudinal, and vertical contact forces of particles in different structural layers are extracted to investigate the interaction between particles in different structural layers under vehicle load. The contact forces between particles are shown in Figs. 19 to 21.

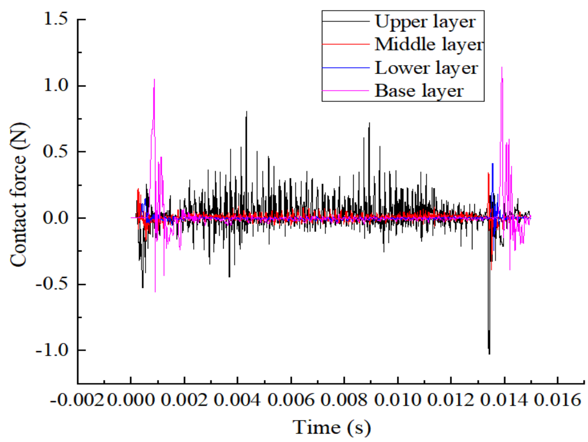

Fig. 19. Transverse contact force of particles.

As shown in Fig. 19, all particles of each structural layer of the road surface bear transverse contact force under the action of vehicle load. The lateral contact force on particles in the upper layer is the highest, ranging from -0.45 N to 0.81 N, and the particles are mainly subjected to tension. When the vehicle load is near or away from the observation point, the contact force of particles is the maximum. When the vehicle load is completely rolled at the observation point, the lateral contact force is small. The transverse contact force of particles in the middle layer is much smaller than that in the upper layer. The lateral contact force between particles in the base layer is the least.

As shown in Fig. 20, the particles in each structural layer of the pavement bear a longitudinal contact force under the action of vehicle load. The upper layer particles are subjected to the maximum longitudinal contact force, which ranges from -0.27 N to 0.231 N. The particles in the upper layer bear both tension and pressure. When the vehicle load is close to the observation point or away from the observation point, the contact force of particles is the maximum. When the vehicle load is completely pressed at the observation point, the longitudinal contact force is small. The longitudinal contact force of particles in the middle layer is much smaller than that of the upper layer. The longitudinal contact force of the base particles is the smallest.

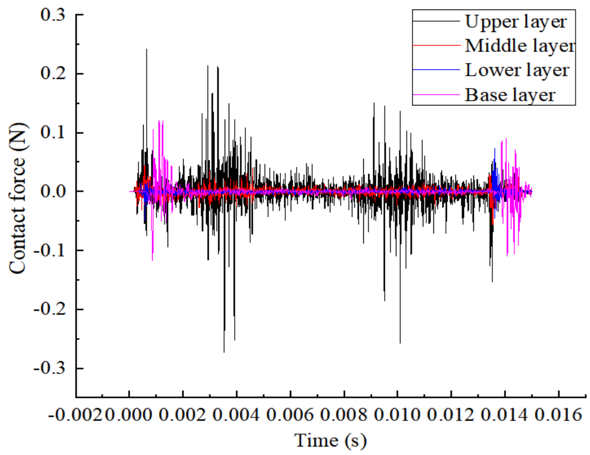

Fig. 20. Longitudinal contact force of particles.

As shown in Fig. 21, the particles in each structural layer of the pavement bear a certain vertical contact force under the action of vehicle load. The curve of the vertical contact force is antisymmetric.

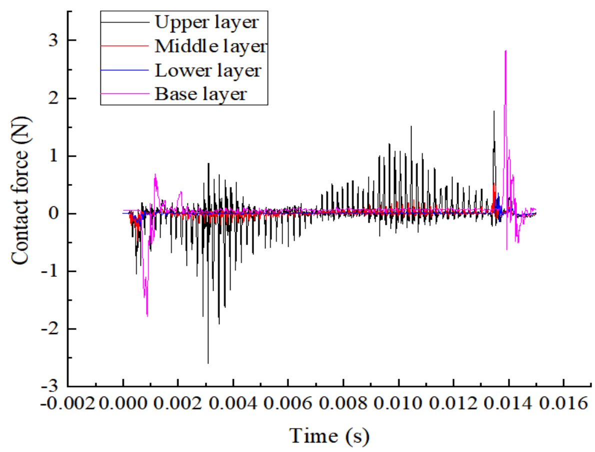

Fig. 21. Vertical contact force of particles.

The vertical contact force of particles in the upper layer is the largest. As the vehicle load gradually approaches the observation point, the vertical contact force of particles gradually increases, reaching a maximum peak value is -2.72 N. When the vehicle load leaves the observation point gradually, the vertical contact force of particles also increases gradually, reaching a maximum peak value of 1.62 N. When the vehicle load is completely pressed at the observation point, the vertical contact force is small. The vertical contact force of particles in the middle layer is much smaller than that of the upper layer. The vertical contact force of the base particles is the minimum.

5. Conclusions

A 1/4 vehicle model and a discrete element model were built to solve for the movement velocity and contact force of the pavement structural layer particles and analyze the movement rule of the particles. The main conclusions are summarized as follows:

(1) The asphalt pavement structure model can be established by using the DEM. The dynamic response of the road surface can be solved by considering the mode of vehicle movement. The error between the calculated results of the discrete element model and the measured results is within 7%. The discrete element model can be used to simulate and analyze the mechanical behavior of vehicles and road surfaces.

(2) Under the action of vehicle loads, the particles of the pavement structure layer exhibit transverse, longitudinal, and vertical movement. The vertical velocity of particles is the largest, and the transverse velocity is the smallest. The velocity of vertical motion is 2.3-2.8 times greater than that of longitudinal motion. The velocity of vertical movement is 5-6 times greater than that of lateral movement. The vertical contact force between particles is the largest, followed by the longitudinal contact force, and the transverse contact force is the least. The longitudinal contact force of particles is 1.5-2 times greater than the transverse contact force.

(3) The translational velocity of particles in the upper layer is much higher than that in the middle layer, and the translational velocity of particles in the base layer is the least. The moving velocity of the particle has both positive and negative values, which indicates that the particle oscillates back and forth. In addition, the particles will rotate around the X, Y, and Z axes. The particle rotates most quickly about the Y axis and least quickly about the Z axis. The rotational velocity of the upper layer particles is much greater than that of the middle layer.

However, the temperature can affect the movement behavior of asphalt particles in actual working conditions. Therefore, the influence of different temperatures on the movement behavior of asphalt particles under vehicle loads will be further studied.

Acknowledgements
This work was financially supported by the Overseas Scholar Program in the Hebei Province (C20190514), and Science and Technology Project of Hebei Province (15457605D, 144576106D), China.

References

1. Coenen, A.R., Kutay, M.E., Sefidmazgi, N.R., Bahia, Hussain. U., “Aggregate structure characterisation of asphalt mixtures using two-dimensional image analysis”. *Road Materials and Pavement Design*, 13(3), 2012, pp. 433-454.
2. Meza-Lopez, J., Norena, N., Meza, C., Romanel, C., “Modeling of asphalt concrete fracture tests with the discrete-element method”. *Journal of Materials in Civil Engineering*, 32(8), 2020, pp. ID 04020228.
3. Li, X.L., Liu, X.Y., Lv, X.C., Zhou, Y.H., “Discrete element analysis of indirect tensile test based on image processing with annular segmentation and bimodal threshold”. *Journal of Testing and Evaluation*, 48(4), 2020, pp. 2750-2767.
4. Zhang, J.P., Tian, H.Q., Pei, J.Z., Qu, T., Liu, W.L., “Evaluating crack resistance of asphalt mixture based on essential fracture energy and fracture toughness”. *International Journal of Geomechanics*, 19(4), 20219, pp. 06019005.
5. Solonenko I., “The use of cement concrete pavements for roads, depending on climatic conditions”. *Technical Journal*, 13(3), 2019, pp. 235-240.
6. Zhang, Y., Ma, T., Ling, M., Zhang, D.R., Huang, X.M., “Predicting Dynamic shear modulus of asphalt mastics using discretized-element simulation and reinforcement mechanisms”. *Journal of Materials in Civil Engineering*, 31(8), 2019, pp. ID 04019163.
7. Arshadi, A., Bahia, H., “Development of an image-based multi-scale finite-element approach to predict mechanical response of asphalt mixtures”. *Road Materials and Pavement Design*, 16, 2015, pp. 214-229.
8. Wang, H., Zhou, Z.H., Huang, W.L., Dong, X.Y., “Investigation of asphalt mixture permanent deformation based on three-dimensional discrete element method”. *Construction and Building Materials*, 272, 2021, pp. ID 121808.
9. Wang, S.R., Xiao, H.G., Zou, Z.S., Cao, C., Wang, Y.H., Wang, Z.L., “Mechanical performances of transverse rib bar during pull-out test”. *International Journal of Applied Mechanics*, 11(5), 2019, pp. ID 1950048.
10. Chen, J.Q, Wang, H., Li, L., “Virtual testing of asphalt mixture with two-dimensional and three-dimensional random aggregate structures”. *International Journal of Pavement Engineering*, 18(9), 2017, pp. 824-836.
11. Miao, Y.H., Yu, W.X., Hou, Y., Guo, L.Y., Wang, L.B., “Investigating the functions of particles in packed aggregate blend using a discrete element method”. *Materials*, 12(4), 2019, pp. ID 556.
12. Li, J., Zhang, J.H., Qian, G.P., Zheng, J.L., Zhang, Y.Q., “Three-dimensional simulation of aggregate and asphalt mixture using parameterized shape and size gradation”. *Journal of Materials in Civil Engineering*, 31(3), 2019, pp. ID 04019004.
13. Ding, X.H., Ma, T., Huang, X.M., “Discrete-element contour-filling modeling method for micromechanical and macro-mechanical analysis of aggregate skeleton of asphalt mixture”. *Journal of Transportation Engineering Part B-Pavements*, 145(1), 2019, pp. ID 04018056.
14. Buttlar, W.G., You, Z.P., “Discrete element modeling of asphalt concrete: microfabric approach”. *Transportation Research Record: Journal of the Transportation Research Board*, 1757, 2001, pp. 111-118.
15. Wang, S.D., Miao, Y.H., Wang, L.B., “Investigation of the force evolution in aggregate blend compaction process and the effect of elongated and flat particles using DEM”. *Construction and Building Materials*, 258, 2020, pp. ID 119674.
16. Chang, M.F., Pei, J.Z., Zhang, J.P., Xing, X.Y., Xu, S.H., Xiong, R., “Quantitative distribution characteristics of force chains for asphalt mixtures with three skeleton structures using discrete element method”. *Granular Matter*, 22(4), 2020, pp. ID 87.

17. Yang, J.H., Wang, S.R., Zhang, H.Q., Cao, C., "Particle-scale analysis of key technologies of the cut-and-cover tunnel on the slope". *Journal of Engineering Science and Technology Review*, 7(4), 2014, pp. 46-52.
18. Wang, S.R., Wang, J.A., Liu, S.H., Wu, S.C., Xie, J.W., "Particle flow analysis on mechanized top-coal caving in steep thick seam". *Journal of University of Science and Technology Beijing*, 28(9), 2006, pp. 802-812.
19. Wu, X.G., Wang, S.R., Yang, J.H., Zhao, J.Q., Chang, X., "Damage characteristics and constitutive model of lightweight shale ceramsite concrete under static-dynamic loading". *Engineering Fracture Mechanics*, 259, 2022, pp. ID 108137.
20. Wang, S.R., Shi, K.P., Zou, Y.F., Zou, Z.S., Wang, X.C., "Size effect analysis of scale test model for high-speed railway foundation under dynamic loading condition". *Tehnicki Vjesnik-Technical Gazette*, 28(5), 2021, pp. 1615-1625.
21. Cheng, Y., Hagan, P., Mitra, R., Wang, S.R., Yang, H.W., "Monitoring failure processes using acoustic emission tomography". *Frontiers in Earth Science*, 9, 2021, pp. ID 765030.
22. Chang, X., Li, Z.H., Wang, S.Y., Wang, S.R., Fu, L., Tang, C.A., "Pullout performances of grouted rockbolt systems with bond defects". *Rock Mechanics and Rock Engineering*, 51, 2018, pp. 861-871.
23. Qian, G.P., Hu, K.K., Li, J., Bai, X.P., Li, N.Y., "Compaction process tracking for asphalt mixture using discrete element method". *Construction and Building Materials*, 235, 2020, pp. ID 117478.
24. Liu, W.D, Gao, Y., Huang, X.M., Li, L.M., "Investigation of motion of coarse aggregates in asphalt mixture based on virtual simulation of compaction test". *International Journal of Pavement Engineering*, 21(2), 2020, pp. 144-156.
25. Ye, Y.L., Sun, Y.Z., Gao, L., Ma, Z., Xue, X.W., "Study on creep behavior of asphalt mixture based on discrete element method". *Baltic Journal of Road and Bridge Engineering*, 15(4), 2020, pp. 174 - 195.
26. Chen, M., Javilla, B., Hong, W., Pan, C.L., Riara, M., Mo, L.T., Guo, M., "Rheological and interaction analysis of asphalt binder, mastic and mortar". *Materials*, 12(1), 2019, pp. ID 128.
27. Li, K.H., Cheng, Y.M., Fan, X., "Roles of model size and particle size distribution on macro-mechanical properties of Lac du Bonnet granite using flat-joint model". *Computers and Geotechnics*, 103, 2018, pp. 43-60.
28. Zhang, Y., Ma, T., Luo, X., Huang, X.M., Lytton, R.L., "Prediction of dynamic shear modulus of fine aggregate matrix using discrete element method and modified Hirsch model". *Mechanics of Materials*, 138, 2019, pp. ID 103148.
29. Sun, X.M., He, M.C., Liu, C.Y., Gu, J.C., Wang, S.R., Ming, Z.Q., Jing, H.H., "Development of nonlinear triaxial mechanical experiment system for soft rock specimen". *Chinese Journal of Rock Mechanics and Engineering*, 24(16), 2005, pp. 2870-2874.